Cell-Specific Multifunctional Processing of Heterogeneous Cell Systems in a Single Laser Pulse Treatment

Ekaterina Y. Lukianova-Hleb,[†] Martin B. G. Mutonga,[†] and Dmitri O. Lapotko[†,‡,*]

[†]Department of Biochemistry and Cell Biology, Rice University, 6100 Main Street, Texas 77005, United States and [‡]Department of Physics and Astronomy, Rice University, 6100 Main Street, Texas 77005, United States

ABSTRACT Current methods of cell processing for gene and cell therapies use several separate procedures for gene transfer and cell separation or elimination, because no current technology can offer simultaneous multifunctional processing of specific cell subsets in highly heterogeneous cell systems. Using the cell-specific generation of plasmonic nanobubbles of different sizes around cell-targeted gold nanoshells and nanospheres, we achieved simultaneous multifunctional cell-specific processing in a rapid single 70 ps laser pulse bulk treatment of heterogeneous cell suspension. This method supported the detection of cells, delivery of external molecular cargo to one type of cells and the concomitant destruction of another type of cells without damaging other cells in suspension, and real-time guidance of the above two cellular effects.

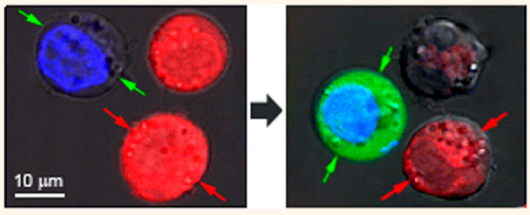

KEYWORDS: delivery · cell separation · graft · laser · plasmonic nanobubble · cell therapy · gold nanoparticle

Most of the cell zand gene therapies that have shown promise against human diseases including cancer require *ex vivo* processing of human cell grafts in order to eliminate unwanted cells from a heterogeneous cell suspension and to genetically modify one or more cell subsets to increase their therapeutic efficacy. Ideally both elimination and transfection should be highly efficient, cell-specific, and fast. Existing methods,[1−29] however, lack such characteristics, especially those of multifunctionality and cellular selectivity when applied to heterogeneous cell systems. As a result, current cell processing for cell and gene therapies is often slow, expensive, and labor intensive and is compromised with high cell losses and poor selectivity, thus limiting the efficacy and availability of these cell therapies.

We considered an entirely new approach that employs the simultaneous transfection of target cells and the elimination of unwanted subsets of other cells in heterogeneous grafts in one procedure with single cell selectivity, high efficacy and processing rates, and low nonspecific toxicity. Such an approach requires efficient mechanisms, cellular agents, and technologies that are not available so far. We therefore evaluated the multifunctional potential of a newly developed class of tunable multifunctional cellular nanoagents, called plasmonic nanobubbles (PNBs).[30−32]

A PNB is not a particle but a transient nanosecond event, a vapor nanobubble that is generated around a gold nanoparticle (NP) after it absorbs a short laser pulse, converts its energy into heat, and evaporates its liquid environment in a nanoexplosive manner (Figure 1). We recently demonstrated that PNBs allow optical detection[32−34] and transmembrane injection of molecular cargo[35−37] and the immediate destruction (elimination) of specific target cells with high speed and selectivity and without collateral damage even when the majority of the cells are nontarget.[32,33,38] The specific function, payload delivery or destruction, is determined by the maximal size of the PNB (Figure 1), which, in turn, is determined by the NP's properties and by the energy of the laser pulse.[30−33] We hypothesized that the ability of each NP type to generate PNBs of different

* Address correspondence to dl5@rice.edu.

Received for review September 29, 2012 and accepted November 20, 2012.

Published online November 20, 2012
10.1021/nn3045243

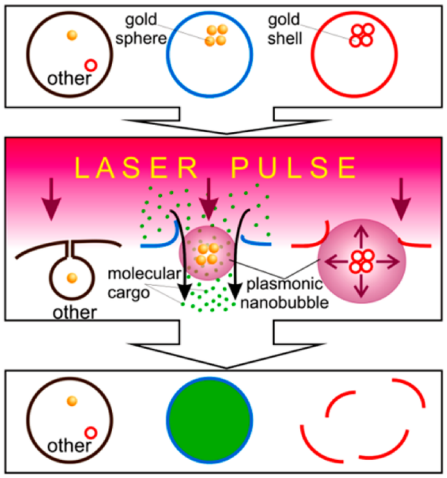

Figure 1. Multifunctional cell-specific processing of a heterogeneous cell system with plasmonic nanobubbles (PNBs) that are selectively generated around the clusters of gold spheres in spheres-targeted cells (*blue*) and around the clusters of gold shells in shells-targeted cells (*red*) with a single laser pulse, resulting in the simultaneous delivery of molecular cargo into blue cells due to injection of the molecules (green dots) with small PNB and mechanical destruction of red cells with large PNB without damage to other cells, all realized in a single pulse treatment.

sizes under identical optical excitation coupled with the cell-specific targeting and clustering of NPs conjugated to cell-specific antibodies would allow the simultaneous transfer of molecular cargo into gold sphere-targeted cells and the destruction of gold shell-targeted cells in a simultaneous bulk treatment of a heterogeneous cell system with high efficacy, speed, and selectivity and with low toxicity (Figure 1). This technology would create a universal platform for cell and gene therapy including stem cell transplantation. To test this hypothesis, we experimentally studied responses of different cells *in vitro* to targeting with specific NP types and to a simultaneous bulk treatment with a single laser pulse that generated PNBs in those cells.

RESULTS

PNB Generation in Gold NP-Treated Cells. The maximal size of a PNB determines its specific cellular effect, destruction or delivery. Large PNBs mechanically destroy cells, while small, noninvasive PNBs inject extracellular molecules into the cell. We initially studied the ability of cells to generate PNBs of two different sizes under exposure to a single laser pulse. Our tasks were to determine how to differentiate the PNB size and to evaluate the cellular specificity of the generation of size-specific PNBs. We applied two NP types with different PNB generation efficacies, 60 nm hollow gold nanoshells (NS) that generate maximal PNBs and 60 nm solid gold spheres (NSP) that generate much smaller PNBs under identical optical excitation conditions.[31] Both NP types were used in plain and OKT3 antibody-conjugated forms (OKT3 antibody

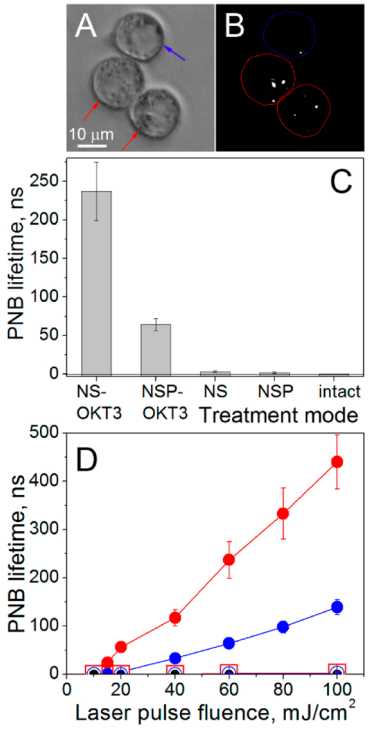

Figure 2. PNBs in cells targeted with gold spheres (NSP) and shells (NS). (A) Bright field image of a mixture of J32 cells treated by NS-OKT3 (*red* arrow) and NSP-OKT3 (*blue* arrow); (B) optical scattering time-resolved image of large (bright) PNBs in NS-OKT3-treated cells (*red*) and small (dim) PNBs in NSP-OKT3-treated cells (*blue*); (C) PNB lifetime in NS-OKT3, NSP-OKT3, NS, NSP-treated, and intact cells, all obtained under exposure to a single laser pulse of 60 mJ/cm^2; (D) PNB lifetime as a function of the laser pulse fluence for NS-OKT3 (*solid red*), NSP-OKT3 (*solid blue*), NS (*hollow red*), NSP (*hollow blue*)-treated and intact (*solid black*) cells.

recognizes CD3 receptor expressed in the employed J32 model cells[35] and is also employed in the clinic for manipulation with human T-cells[36,37]). The NS-OKT3-targeted J32 cells (CD3-positive) were labeled with red fluorescent marker (Calcein Red AM), and the NSP-OKT3-targeted J32 cells were labeled with blue fluorescent marker (DAPI) for their identification through fluorescent imaging. After incubating the cells for one hour with each type of NPs, the cells were mixed (Figure 2A) and individual cells were exposed to a single laser pulse (70 ps, 532 nm) of a specific fluence above the PNB generation threshold in order to generate and detect PNBs.

Transient PNBs in individual cells were detected and imaged with time-resolved optical scattering imaging by using a pulsed probe laser. The light scattered by the PNBs produced their bright images (Figure 2B). The maximal diameter of the PNB was measured in individual cells as the duration of the PNB-specific optical scattering time response[31] (Figure 3B) that was obtained with an additional continuous probe laser. PNB lifetimes were analyzed for five cell populations under identical optical excitation: intact cells, cells incubated with plain NSs and NSPs, and cells incubated with

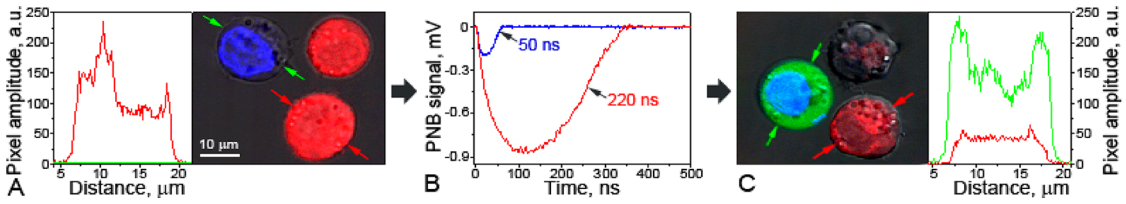

Figure 3. (A) J32 cells with intracellular clusters of gold spheres (NSP-OKT3, blue DAPI marker) and shells (NS-OKT3, Calcein Red marker); (B) optical scattering PNB-specific time responses of individual cells to a single laser pulse show simultaneous generation of small PNBs in blue and large PNBs in red cells in the presence of extracellular molecular cargo FITC- Dextran (the lifetimes of PNBs are shown); (C) postlaser treatment blue cells show the injected FITC-Dextran (*green* fluorescence), and red cells show leaked out Calcein Red dye and distorted membranes due to their destruction. The fluorescence intensity profiles of individual cells in (A) and (C) are indicated by small color-matched arrows.

OKT3-conjugates of NSs and NSPs (Figure 2C). In the range of laser pulse fluence between 10 mJ/cm^2 (close to the PNB generation threshold) and 100 mJ/cm^2 we observed PNBs only in cells treated with OKT3-conjugated NPs (Figure 2C, D). Intact cells or cells incubated with plain NPs did not produce any PNBs at all because the PNB generation threshold in those cells was apparently higher than the laser fluence applied. In contrast, the cells incubated with the same NPs conjugated to the CD3-specific antibody OKT3 showed a 92−96% probability of PNB generation because their PNB generation threshold fluences were lower than the fluence applied. Such a significant reduction in the PNB generation threshold fluence (compared to cells targeted with plain NPs) was caused by the formation of large intracellular clusters of NPs through the mechanism of the receptor-mediated endocytosis.[38−42] We have found earlier that an increase in the NP cluster size reduces the PNB generation threshold fluence, which will be minimal for large intracellular NP clusters and maximal for single nonspecifically taken NPs.[30,31] Thus, the receptor-mediated endocytosis of NP-OKT3 created the largest NP clusters in CD3-positive cells and enabled the selective generation of PNBs under exposure to laser pulses of low fluence level starting at 10−15 mJ/cm^2 (Figure 2D).

Influence of NP Properties on PNB Size. Next, we observed the difference in PNB size (lifetime) of the NS-OKT3- and NSP-OKT3-targeted cells under identical targeting and optical excitation conditions (Figure 2C). The PNB lifetime was found to be NP type-specific: NS-OKT3-targeted cells yielded relatively large PNBs with lifetimes of 200−300 ns, while NSP-OKT3-targeted cells developed 3- to 4-fold smaller PNBs with lifetimes of 50−75 ns. This NP type-specific difference in PNB size was caused by the difference in the PNB generation efficacy of NSs (high) and NSPs (low) due to the difference in heat capacity of a NS (low) and a NSP (high).[31] Specifically, the low heat capacity of a NS (compared to an NSP of the same diameter) provides faster and more efficient transfer of the thermal energy from the heated metal to an adjacent water. A NS also consumes much less energy for the internal heating compared to a solid NSP.

A significant difference in the PNB lifetimes of NS-OKT3-targeted and NSP-OKT3-targeted cells was observed in a wide range of the excitation laser fluences between 10 and 100 mJ/cm^2 (Figure 2D). Furthermore, the PNB lifetime almost linearly increased with the fluence above the PNB generation thresholds, which were found to be approximately 15 mJ/cm^2 for NS-targeted cells and about 40 mJ/cm^2 for NSP-targeted cells. Therefore, PNB size (which determines the specific cellular effect of the PNB) can be precisely tuned with the fluence of the laser pulse. In particular, the PNB size for NS-OKT3- and NSP-OKT3-targeted cells can be adjusted to the desired range by simply varying the laser fluence.

These results demonstrate that two specific antibody-conjugated types of gold NPs with different PNB-generating efficacies, hollow gold nanoshells and solid gold nanospheres, provide the generation of PNBs of two sizes with a 4-fold difference under identical simultaneous excitation. Next we evaluated the cellular effects on the NS- and NSP-induced PNBs.

Bulk PNB Treatment of a Heterogeneous Cell System with a Single Laser Pulse. The heterogeneous cell system was modeled by mixing NSP-OKT3-targeted and NS-OKT3-targeted J32 cells that modeled human T-lymphocytes. NSP-OKT3-targeted cells were labeled with blue fluorescent marker (DAPI) to identify the cells and their nuclei, and NS-OKT3-targeted J32 cells were labeled with red fluorescent marker (Calcein Red) to identify the cells and to monitor their integrity and viability after PNB generation.[43] Then the blue and red cells were mixed into one suspension to model a heterogeneous cell system, and green fluorescent dye (FITC-Dextran) was added to the cell suspension as a model of the molecular cargo. Next, the suspension was scanned with a broad (0.22 mm diameter) excitation laser beam for the bulk PNB treatment. The broad laser beam simultaneously and identically irradiated hundreds of mixed red and blue cells in one pulse. All the cells received a single pulse exposure. We used the above data (Figure 2D) to set the pulse fluence to the level of 60 mJ/cm^2, which corresponds to the PNB lifetime of 60−65 ns in NSP-OKT3-treated cells and 200−220 ns in NS-OKT3-treated cells. After the laser

irradiation, FITC-Dextran was immediately washed off. The experiment was performed in three steps: (1) fluorescent imaging of the mixed cells before exposure to FITC-Dextran and the laser, (2) adding FITC-Dextran and exposing the cells to broad single laser pulses that induced PNBs, and (3) fluorescent imaging of the cells immediately after the PNB treatment.

Prior to the PNB treatment we obtained tricolor confocal fluorescent images of the cells (Figure 3A) and measured the levels of red (to characterize the viability) and green (to characterize the presence of the external cargo) fluorescence in individual cells. The viability of the cells was measured by monitoring the level of Calcein Red fluorescence[43] and with the Trypan Blue exclusion test. Treatment of the cells with a single laser pulse of the fluence of 60 mJ/cm^2 provided the generation of 64 $\pm$ 8 ns PNBs in blue cells and 237 $\pm$ 38 ns PNB in red cells (Figure 3B) and resulted in a significant increase in green fluorescence of FITC-Dextran only in the blue cells and in a significant decrease of red fluorescence of Calcein Red in the red cells (Figure 3C). Blue NSP-OKT3-targeted cells showed the presence of FITC-Dextran in their cytoplasm (Figure 3C), which was not found there before the PNB treatment (Figure 3A). Intracellular delivery of FITC-Dextran was achieved through the PNB-specific mechanism of the localized injection of the extracellular molecules. We recently demonstrated that a small PNB of 40−90 ns lifetime creates a small transient hole in the cellular membrane and induces a nanojet that actively injects the external molecules into the cytoplasm without compromising the cell.[38,39] Comparison of the concentration and viability of the blue cells before and after the PNB treatment showed that such small PNBs (64 ns) were relatively safe to the cells (Figure 4).

Red (NS-OKT3-targeted) cells showed a totally different response to the same laser pulse that induced much larger PNBs (237 $\pm$ 38 ns) (Figure 3B). Calcein Red apparently leaked out, and the shape of the cells changed, showing the blebbing bodies and damaged membrane in the bright field image (Figure 3C). A comparison of the concentration and viability of the red cells before and after the PNB treatment showed that such large PNBs destroyed 86% of these cells (Figure 4). The PNB-induced changes in the cell shape, level of red fluorescence, cell concentration, and viability were observed within 10 min after the PNB treatment. The character and speed of these changes indicate that cell death occurred simultaneously through a lysis-like process and not through necrosis or apoptosis. Such an immediate cell death effect was caused by the mechanical explosive action of a large intracellular PNB and not by laser-induced heating of gold NPs because PNBs effectively insulate the thermal effect of gold NPs.[31] Our recent detailed study of the PNB-induced cell death mechanism revealed the disruptive irreversible damage

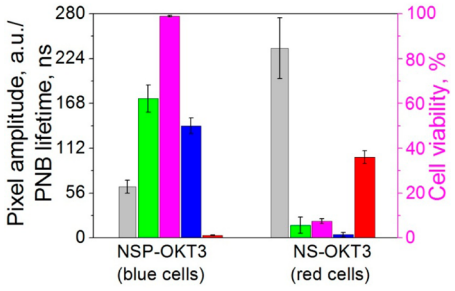

Figure 4. Parameters of individual red and blue cells targeted with NS-OKT3 and NSP-OKT3, respectively, after a single laser pulse treatment with PNBs (normalized by the corresponding parameters before the laser pulse): PNB lifetime (*gray*), cell destruction (shown through the viability level, *magenta bars*), and cargo delivery (shown through the level of green fluorescence, *green bars*); two types of gold NP-targeted cells are identified through the fluorescence of their markers, blue and red.

of the cell structure after generating even a single large intracellular PNB.[32]

It should be noted that a small fraction of the red cells also showed an increase in green fluorescence due to the incidental entry of the extracellular FITC-Dextran into the cells with disrupted membranes (Figure 4). The level of intracellular green fluorescence in red cells was much lower than that in blue cells. Unlike the blue cells, the disrupted red cells with compromised membranes were unable to keep the injected cargo, and it rapidly leaked out together with Calcein Red. Also, based on the significant drop in the concentration of red cells, it appears that many red cells were destroyed to a level that showed no cell image at all due to their full destruction by PNBs and the following elimination of their debris during washing off the FITC-Dextran dye.

This experiment demonstrates a simultaneous activation of two different cellular functions of PNBs, the noninvasive delivery of molecular cargo and the destruction of cells. In addition, we observed a single cell selectivity of both functions in a heterogeneous cell suspension. Finally, these two functions were rapidly administered in a single laser pulse bulk treatment of multiple cells in less than a nanosecond. Such high efficacy, selectivity, and speed were provided by the high cellular specificity of PNBs and their on-demand mechanical (not thermal) mechanisms of cell destruction and cargo delivery. Such multifunctional and selective processing of a heterogeneous cell system in a single bulk treatment was never achieved beforehand with existing cell processing methods.

Cell Detection and Real-Time Guidance. Finally, we correlated the optically detected lifetimes of PNBs to the metrics of their delivery and destruction efficacy for individual cells (Figure 4). Delivery was quantified through the cell-averaged pixel image amplitude of green, FITC-specific fluorescence. Destruction was quantified through the relative change in the cell

concentration and viability measured within 10 minutes after the PNB treatment. We found a strong correlation between the detected PNB lifetime, the cell type, and specific cellular function, delivery or destruction (Figure 4). A short PNB lifetime was associated with the blue cells and with the noninvasive delivery of extracellular molecules (an increase in green fluorescence, no decrease in cell concentration and viability). In contrast, a long PNB lifetime was associated with the red cells and with cell destruction (a decrease in Calcein Red fluorescence level, cell concentration, and viability). This result showed two additional functions of PNBs, which are the cell detection and the real-time guidance of the cell processing. Since the optical time responses of PNBs (or other signals such as images (Figure 2A) or acoustic responses[38]) can be obtained for individual cells, such detection and guidance can be performed in real time. Therefore, continuous monitoring of PNBs during the processing of a heterogeneous cell system allows real-time adjustment of the fluence of laser pulses in order to maintain desired PNB lifetimes even when the PNB generation conditions in cells vary. The detection and processing of the PNB signal requires microseconds, and electro-optical modulators allow the adjustment of the laser fluence in milliseconds, thus allowing cell processing at laser pulse repletion rates of up to 100 Hz and cell processing rates of up to 10^{8-9} cells per minute.

DISCUSSION

Comparison of the PNB Mechanisms with Current Approaches. Current methods of cell processing for gene and cell therapies use several separate procedures for gene transfer and cell elimination, because no current technology can offer simultaneous multifunctional processing of different specific cells in highly heterogeneous cell systems. Our first major innovation is to use a single process with multiple functions to simultaneously engineer one target cell subset, eliminate a second, and leave the nonspecific bulk cells unmodified. The second innovation is in providing single cell selectivity and a high speed of cell processing in heterogeneous cell systems.

Cell elimination (separation) methods use physical and affinity criteria such as filtering, centrifuging, fluorescent-activated flow sorting, and magnetic and adsorbent removal of target cells. The best results were achieved with target-specific antibodies conjugated to either magnetic beads or biotin to bind to the target cells and then to pass through columns to select the target cells (for example CD34+ stem cells[1,2]). When applied to human grafts, the limitations of immunotargeting include the incomplete removal of contaminating cancer cells or the removal of important immune cells[1,2] as well as a lack of selectivity due to the unavoidable nonspecific binding of antibodies to nontarget cells.[1,2] None of these technologies can provide the optimal combination of efficacy, selectivity, processing rate, and low toxicity.

Current cell transfection methods are similarly limited. Three major approaches deliver plasmids with viral,[3−5] nonviral using plasmid carriers,[6−11] and nonviral using external energy[6,12−24] methods. While viruses offer greater efficacy of gene transfer, nonviral methods provide better safety and are usually less immunogenic. Carrier-based approaches use liposomes, dendrimers, polyplexes, polyethyleneimine, and other NPs. Of these methods, lipofection (liposomes as carriers) is widespread.[9,44,45] Use of plasmid carriers improves the efficacy and safety of gene transfer,[8−11,46−50] but the selectivity of such methods in heterogeneous cell suspensions is limited by the nonspecific uptake of carriers by nontarget cells. PNBs with their much higher cellular specificity overcome this limitation.[34] In addition, PNBs rapidly deliver the cargo within nanoseconds, improving both processing rates and reducing the toxicity of the delivery procedure compared to slow diffusion-based current methods.

External energy-based methods use sono-, electro-, and optoporation of cells,[12−24] of which electroporation/nucleofection is most widely used,[12] despite its poor selectivity and cellular toxicity. Gene transfer also employs laser methods through heating, shockwave generation optical breakdown, and bubble generation.[18−20,22−24,51−53] The bubbles originate from external thermal or cavitation sources, and thus they cannot discriminate target from nontarget cells. All current laser methods do not provide cell selectivity in heterogeneous cell systems. Moreover, almost all external energy-based methods also depend on the slow diffusion of plasmids through the entry point produced in the cell membrane. Rapid active delivery through optoinjection can be achieved by using femtosecond laser pulse-induced optical breakdown,[20,21,23] but requires the precise positioning of the laser beam on an individual target cell and therefore cannot be used for bulk treatment with high processing rates.

Contrary to the above limitations, we demonstrated several innovative properties of PNBs: (1) high cellular specificity (10−20-fold better than that of NPs; see Figure 4) due to the cluster-threshold PNB mechanism that prevents the generation of PNBs in nontarget cells under simultaneous optical excitation of many target and nontarget cells;[3,5] (2) active nanosecond mechanical, nonthermal, and reagent-free mechanisms of either delivery of molecular cargo or cell destruction that provide cell treatment of the highest precision;[34,35,38] (3) low collateral biodamage due to the localized nature of PNBs and the reduction in the doses of optical energy and NPs by 3 to 6 orders of magnitude. The major innovation is in combining the above four functions in one rapid procedure. Such four-in-one functionality is not supported by any other technologies

taken alone. In addition, the injection mechanism supported by PNB is very transient and localized[39] because it mechanically, nonthermally, impacts the membranes of specific target cells. On the basis of the hydrodynamics of PNB we earlier estimated that the size and the lifetime of the transient hole (pore) in the cellular membrane are comparable to those of a PNB, *i.e.*, are less than 1 μm and 1 μs, respectively. The mechanical nature of the PNB impact can be explained through the physical mechanism of a PNB generation. Unlike stationary photothermal conversion of the continuous optical radiation by gold NPs,[53] PNBs are generated through a very nonstationary photothermal process upon the absorption of a 70 ps single laser pulse. This creates the intense localized heating of the adjacent to the NP water and supports the most efficient localized vapor generation. While the transient laser-induced temperature of the NP may reach 700−1000 K, as we recently modeled for the same laser pulse and 60 nm gold spheres,[57] the vapor inside the PNB efficiently thermally insulates its outer environment from such extreme heating, resulting in almost ambient outer temperature.[31] In this case the impact of a PNB has a purely mechanical nature and is determined by the expansion and collapse of a PNB that can be quantified through its maximal diameter or the lifetime.[31]

Applications. The multifunctionality, selectivity, and speed of the described PNB method will find several clinical applications for cell and gene therapy and stem cell or bone marrow transplantation. The ability to simultaneously genetically modify target cells (like T-cells) and eliminate unwanted cells (like regulatory T-cells) from a highly heterogeneous graft, with single cell selectivity and without compromising other important accessory cells, will enhance the effectiveness of cell engineering in general and gene therapies in particular. The technology may subsequently be applied to process any liquid tissues to improve the outcome of other cell-based interventions in cancer and other disorders. The high speed of the PNB mechanisms coupled with the broad laser beam (available with commercial lasers) will enable a cell processing rate of up to 10^9 cells per minute, which will meet clinical requirements for cell processing.

CONCLUSIONS

Using the cell-specific generation of plasmonic nanobubbles of two different sizes we achieved a simultaneous multifunctional cell-specific processing in a rapid single pulse procedure in a heterogeneous cell suspension. Single laser pulse bulk treatment of multiple heterogeneous cells showed high efficacy and selectivity in both the delivery of molecular cargo and cell destruction without damaging nontarget cells. The optical detection of PNBs enabled two additional functions of the detection of specific target cells and of a real-time guidance of their processing. None of the existing methods of cell processing can provide such simultaneous and cell-specific multifunctionality. Thus the developed PNB method supports four functions in a single laser pulse procedure: cell detection, delivery of molecular cargo, cell destruction, and the guidance of delivery and destruction.

MATERIALS AND METHODS

Gold NPs and Their Conjugation. We used two types of gold NPs: 60 nm gold spheres and 60 nm hollow gold nanoshells. NSPs were obtained from BioAssayWorks LLC (Ijamsville, MD, USA). NSs were synthesized by galvanic replacement of gold on a silver core.[54] The advantages of this type of NP include low toxicity, reliable conjugation properties, and high PNB generation efficacy. For active targeting and endocytosis, the NPs were covalently conjugated to OKT3 antibody by BioAssayWorks LLC (Ijamsville, MD, USA). Both NP conjugates were stored in 0.1× PBS and 0.5% (w/v) BSA. The latter prevented a spontaneous clustering of gold NPs in solution.

Cell Model. *Targeting Cells with Gold NPs.* CD3-positive Jurkat (J32) T-cell leukemia cells were employed to model human CD3-positive T-lymphocytes that are clinically used for cell therapy applications with OKT3 antibody. J32 cells are very similar to human lymphocytes in terms of their targeting. J32 cells were targeted with plain and covalently conjugated gold NPs (NSP and NS). Cells (2×10^6 cell/mL) were resuspended in a serum-free RPMI-1640 medium (Invitrogen, Grand Island, NY, USA) containing NPs at a concentration of 5.3×10^9 particles/mL and incubated with the NP-containing media for one hour at 37 °C in a CO_2 incubator. Following incubation, the cells were washed twice to remove unbound NPs and finally suspended in RPMI-1640 medium supplemented with 10% fetal bovine serum (Atlanta Biologicals, Lawrenceville, GA, USA), 2 mM l -glutamine, 100 units/mL penicillin, and 100 mg/mL streptomycin (Life Technologies, Inc., Grand Island, NY, USA). Four different samples of J32 cells were prepared: cells treated with NSP-OKT3 conjugates, with NS-OKT3, and with plain NSPs and NSs. Cells were cultured in Ibidi μ-Slides (#81506, Ibidi, LLC, Verona, WI, USA).

Cell Identification and Monitoring. For the identification of individual cells in the heterogeneous sample of J32 cells treated with NSP-OKT3 and NS-OKT3, we used two different fluorescent dyes: CellTrace Calcein Red AM (C34851, Invitrogen Corporation, Carlsbad, CA, USA) and DAPI (D1306, Molecular Probe Inc., Eugene, OR, USA). Cells treated with NSP-OKT3 were incubated with DAPI (one hour at room temperature), and cells incubated with NS-OKT3 were stained with Calcein Red (one hour with 5 μM of Calcein at 4 °C). After that, both of the samples were mixed in the proportion 1:2, and the heterogeneous sample of blue and red J32 cells was used for bulk treatment with a single laser pulse.

Molecular Cargo. Fluorescence dye FITC-Dextran (2 mg/mL, mol wt 10 kDa) was added to the heterogeneous sample of blue and red J32 cells just prior to their exposure to laser pulses and was washed three times with fresh media after the PNB generation. To ensure that optical absorption of the laser pulse by FITC-Dextran in cells will not influence the PNB generation, we experimentally verified that no vapor nanobubbles were generated due to absorption of the excitation laser pulses by FITC. To avoid bleaching problems with FITC, we employed a single picosecond pulse with a very low total optical dose (60 mJ/cm^2) that practically did not cause any problems with detecting the FITC fluorescence in cells.

Cell Characterization. The cell concentration and viability were tested before and after the PNB treatment of cell suspensions. The standard indicators were used for monitoring the viability of individual cells: CellTrace Calcein Red AM and Trypan Blue. The first dye is well retained by live cells that possess intact plasma membranes, and consequently it is a useful fluorescent tracer and indicator of cell viability and integrity.[43] Thus this dye was used for labeling of J32 cells incubated with NS-OKT3 and for monitoring their integrity, *i.e.*, the potential leakage of the cellular content after PNB treatment.

Individual living cells were assayed with a laser confocal microscope (LSM-710, Carl Zeiss MicroImaging GmbH, Germany) in bright field and three fluorescent (for imaging of Calcein Red, DAPI, and FITC-Dextran) modes. The mean pixel image amplitude of the fluorescent image was measured for individual cells and then averaged for the subpopulation studied (50 cells in total). Cells were considered as Calcein Red AM-, DAPI-, or FITC-Dextran-positive when their image pixel amplitude exceeded that of intact cells. The averaged values of the pixel image amplitudes of each subpopulation of cells were obtained prior to and after the PNB generation.

The viability of cells targeted with NS-OKT3 after PNB treatment was calculated as the concentration of Calcein Red AM-positive target cells before (C_0) and after (C_1) treatment: $V = C/C_1 \times 100\%$.

As an additional viability test, we used Trypan Blue staining for each cell sample before and after separate PNB treatment under conditions identical to the processing of the mixed sample of red and blue J32 cells. To evaluate the efficacy of the PNB cell treatment, we used one complex parameter that combined the changes in cell concentration and viability and calculated from the level of cell viability and concentration: $RRV = C_2/C_0 \times V_l$, where C_2 is cell concentration after treatment, C_0 is the initial cell concentration before treatment, and V_l is the viability of the cells measured after PNB treatment.

PNB Generation and Detection. A PNB is a vapor nanobubble (Figure 5A) transiently induced around a superheated intracellular gold NP cluster upon absorption of a short laser pulse. Gold NPs convert optical energy into heat through the mechanism of plasmon resonance,[55,56] which evaporates the surrounding liquid. Upon the onset of a vapor nanobubble the latter insulates the high NP temperature from its outer environment, whose temperature remains practically ambient.[31] Therefore, the outer effect of a PNB has a mainly mechanical, not thermal, nature, which is determined by the PNB expansion and collapse. The biological function of a PNB is determined by its maximal size, which is measured through the PNB lifetime[31] (Figure 5B). PNBs were generated by transient heating of gold NPs with single laser pulses to temperatures well above the evaporation threshold for the liquid environment of NPs. We employed a single 70 ps pulse at the wavelength of 532 nm (PL-2250, Ekspla, Vilnius, Lithuania), with an optical absorbance spectrum maximum very close to the laser wavelength.

We used previously developed methods and experimental setup[31,32] to generate, image, detect, and quantify PNBs in individual cells through their optical scattering images and time responses detected in parallel with two probe lasers (Figure 5). The shape of the time response signal was specific and different for a heating−cooling effect without generation of a PNB and for generation of a PNB, while the duration of the PNB-specific response characterized the PNB lifetime. The maximal diameter of a PNB is proportional to the PNB lifetime.[30,31,38] In addition, the excellent optical scattering properties of the PNB[32−34] were used for its imaging in cells with the second pulsed probe beam (576 nm, 70 ps, 0.1 mJ/cm^2). This beam was directed at the sample under a high angle of incidence and with 10 ns delay relative to the excitation laser pulse. Thus only the light scattered by the transient PNB was collected by the microscope objective (20×) and detected by the imaging device described above. The diameter of the pump (excitation) laser beam was 220 μm for PNB generation in monolayers of blue and red J32 cells in scanning mode. The fluence was applied in the range 10−100 mJ/cm^2 and was measured by registering its image and measuring the beam diameter at the sample plane with an imaging device (Luka, Andor Technology, Northern Ireland) and by measuring the pulse energy using a pulse energy meter (Ophir Optronics, Ltd., Israel). This scheme provided direct and precise measurements of the incident optical fluence at the cell plane for each excitation pulse. The fluence was controlled through the polarizing attenuator. Operation of all hardware was controlled by a PC through custom software modules developed using the LabView platform.

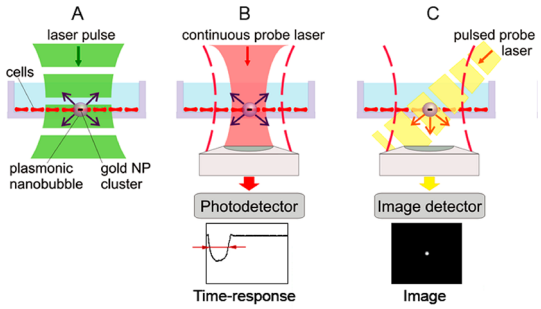

Figure 5. Experimental setup for the excitation and detection of plasmonic nanobubbles with two simultaneous techniques. (A) Generation of a vapor nanobubble around a gold NP cluster inside the cell. (B) Optical scattering response is obtained with a continuous probe laser (633 nm) that is focused into a sample collinearly with the excitation pulse. The scattering effect of the nanobubble reduces the axial intensity of the probe beam, which is measured by a fast photodetector. (C) Time-resolved optical scattering imaging employs side illumination with a probe laser pulse (70 ps, 580 nm, 2 nJ) that is delayed for 10 ns relative to the excitation pulse. The probe light is scattered by the water−vapor boundary of the nanobubble and generates a distinct image in the microscope.

Conflict of Interest: The authors declare no competing financial interest.

Acknowledgment. The authors thank Prof. Malcolm Brenner of Gene and Cell Therapy Center (Houston, TX, USA) for his help with the design of the cell model and for valuable scientific discussions. J32 cells were kindly supplied by Prof. Leonid Metelitsa of Texas Children's Hospital (Houston, TX, USA). This work was supported in part by National Institutes of Health Grant R01GM094816. Confocal microscopy was performed on equipment obtained through a Shared Instrumentation Grant from the National Institutes of Health (S10RR026399-01).

REFERENCES AND NOTES

1. Holmberg, L. A.; Boeckh, M.; Hooper, H.; Leisenring, W.; Rowley, S.; Heimfeld, S.; Press, O.; Maloney, D. G.; McSweeney, P.; Corey, L.; *et al.* Increased Incidence of Cytomegalovirus Disease after Autologous CD34-Selected Peripheral Blood Stem Cell Transplantation. *Blood* **1999**, *94*, 4029–4035.
2. Rutella, S.; Rumi, C.; Laurenti, L.; Pierelli, L.; Sora, F.; Sica, S.; Leone, G. Immune Reconstitution After Transplantation of Autologous Peripheral CD34+ Cells: Analysis of Predictive Factors and Comparison with Unselected Progenitor Transplants. *Br. J. Hamaetol.* **2000**, *108*, 105–115.
3. Kreppel, F.; Kochanek, S. Modification of Adenovirus Gene Transfer Vectors with Synthetic Polymers: a Scientific Review and Technical Guide. *Mol Ther.* **2008**, *16*, 16–29.
4. Pfeifer, A.; Verma, I. M. Gene Therapy: Promises and Problems. *Annu. Rev. Genomics Hum. Genet.* **2001**, *2*, 177–211.
5. Roesler, J.; Brenner, S.; Bukovsky, A. A.; Whiting-Theobald, N.; Dull, T.; Kelly, M.; Civin, C. I.; Malech, H. L. Third-Generation, Self-inactivating gp91 (phox) Lentivector Corrects the Oxidase Defect in NOD/SCID Mouse-Repopulating Peripheral Blood-Mobilized CD34+ Cells from Patients with X-linked Chronic Granulomatous Disease. *Blood* **2002**, *100*, 4381–4390.
6. Kim, T. K.; Eberwine, J. H. Mammalian Cell Transfection: the Present and the Future. *Anal. Bioanal. Chem.* **2010**, *397*, 3173–3178.

7. Rogers, M. L.; Rush, R. A. Non-viral Gene Therapy for Neurological Diseases, with an Emphasis on Targeted Gene Delivery. *J. Controlled Release* **2012**, *157*, 183–189.
8. Torchilin, V. Liposomes in Drug Delivery. In *Fundamentals and Applications of Controlled Release Drug Delivery. Advances in Delivery Science and Technology;* Siepmann, J.; Siegel, R.A.; Rathbone, M. J.,Eds.; Springer US: New York, 2012; Part 4, pp 289−328.
9. Felgner, P. L.; Gadek, T. R.; Holm, M.; Roman, R.; Chan, H. W.; Wenz, M.; Northrop, J. P.; Ringold, G. M.; Danielsen, M. Lipofection: A Highly Efficient, Lipid-Mediated DNA-Transfection Procedure. *Proc. Natl. Acad. Sci. U. S. A.* **1987**, *84*, 7413–7417.
10. Hunt, M. A.; Currie, M. J.; Robinson, B. A.; Dachs, G. U. Optimizing Transfection of Primary Human Umbilical Vein Endothelial Cells Using Commercially Available Chemical Transfection Reagents. *J. Biomol. Technol.* **2010**, *21*, 66–72.
11. Musacchio, T.; Torchilin, V. P. Recent Developments in Lipid-based Pharmaceutical Nanocarriers. *Front. Biosci.* **2011**, *16*, 1388–1412.
12. Scheibe, F.; Gladow, N.; Mergenthaler, P.; Tucker, A. H.; Meisel, A.; Prockop, D. J.; Priller, J. Nonviral Gene Delivery of Erythropoietin by Mesenchymal Stromal Cells. *Gene Ther.* **2012**, *19*, 550–560.
13. Fechheimer, M.; Boylan, J. F.; Parker, S.; Sisken, J. E.; Patel, G. L.; Zimmer, S. G. Transfection of Mammalian Cells with Plasmid DNA by Scrape Loading and Sonication Loading. *Proc. Natl. Acad. Sci. U. S. A.* **1987**, *84*, 8463–8467.
14. Paliwal, S.; Bankiewicz, K. S.; Bringas, J. R.; Heart, G.; Mitragotri, S.; Prausnitz, M. R. Ultrasound-Enhanced Drug Transport and Distribution in the Brain. *AAPS Pharm. Sci. Tech.* **2010**, *11*, 1005–1017.
15. Paliwal, S.; Mitragotri, S. Ultrasound-Induced Cavitation: Applications in Drug and Gene Delivery. *Expert Opin. Drug Delivery* **2006**, *3*, 713–726.
16. Qiu, Y.; Luo, Y.; Zhang, Y.; Cui, W.; Zhang, D.; Wu, J.; Zhang, J.; Tu, J. The Correlation between Acoustic Cavitation and Sonoporation Involved in Ultrasound-Mediated DNA Transfection with Polyethylenimine (PEI) *in Vitro*. *J. Controlled Release* **2010**, *145*, 40–48.
17. Choi, Y.; Yuen, C.; Maiti, S. N.; Olivares, S.; Gibbons, H.; Huls, H.; Raphael, R.; Killian, T. C.; Stark, D. J.; Lee, D. A.; *et al*. A High Throughput Microelectroporation Device to Introduce a Chimeric Antigen Receptor to Redirect the Specificity of Human T Cells. *Biomed. Microdevices* **2010**, *12*, 855–863.
18. Tsukakoshi, M.; Kurata, S.; Nomiya, Y.; Ikawa, Y.; Kasuya, T. A Novel Method of DNA Transfection by Laser Microbeam Cell Surgery. *Appl. Phys. B: Laser Opt.* **1984**, *35*, 135–140.
19. Schomaker, M.; Baumgart.; Ngezahayo, J.; Bullerdiek, A.; Nolte, J.; Escobar, I.; Lubatschowski, H. M.; Heisterkamp, H. A. Plasmonic Perforation of Living Cells Using Ultrashort Laser Pulses and Gold Nanoparticles. *Proc. SPIE* **2009**, *7192*, 71920U.
20. Stevenson, D.; Agate, B.; Tsampoula, X.; Fischer, P.; Brown, C. T. A.; Sibbett, W.; Riches, A.; Gunn-Moore, F.; Dholakia, K. Femtosecond Optical Transfection of Cells: Viability and Efficiency. *Opt. Express* **2006**, *14*, 7125–7133.
21. Vogel, A.; Noack, J.; Huttman, G.; Paltauf, G. Mechanisms of Femtosecond Laser Nanosurgery of Cells and Tissues. *Appl. Phys. B: Laser Opt.* **2005**, *81*, 1015–1047.
22. Dijkink, R.; Le Gac, S.; Nijhuis, E.; van den Berg, A.; Vermes, I.; Poot, A.; Ohl, C. D. Controlled Cavitation-Cell Interaction: Trans-Membrane Transport and Viability Studies. *Phys. Med. Biol.* **2008**, *53*, 375–390.
23. Kohli, V.; Acker, J. P.; Elezzabi, A. Y. Reversible Permeabilization Using High-Intensity Femtosecond Laser Pulses. *Biotechnol. Bioeng.* **2005**, *92*, 889–899.
24. Chakravartu, P.; Qian, W.; El-Sayed, M.; Prausnitz, M. Delivery of Molecular into Cells Using Carbon Nanoparticles Activated by Femtosecond Laser Pulses. *Nat. Nanotechnol.* **2010**, *5*, 607–611.
25. Yang, L.; Kang, W. K. The Effect of HIF-1alpha siRNA on Growth and Chemosensitivity of MIA-paca Cell Line. *Yonsei Med. J.* **2008**, *49*, 295–300.
26. Yang, H.; Robinson, S. N.; Nieto, Y.; Jones, R. J.; Gocke, C. D.; Lu, J.; Giralt, S. A.; Jones, R. B.; Decker, W. K.; Xing, D.; *et al*. *Ex Vivo* Graft Purging and Expansion of Autologous Blood Progenitor Cell Products from Patients with Multiple Myeloma. *Cancer Res.* **2011**, *71*, 5040–5049.
27. Yang, H.; Eaves, C.; de Lima, M.; Lee, M. S.; Champlin, R. E.; McMannis, J. D.; Robinson, S. N.; Niu, T.; Decker, W. K.; Xing, D.; *et al*. A Novel Triple Purge Strategy for Eliminating Chronic Myelogenous Leukemia (CML) Cells from Autografts. *Bone Marrow Transplant.* **2006**, *37*, 575–582.
28. Zhao, N.; Qi, J.; Zeng, Z.; Parekh, P.; Chang, C. C.; Tung, C. H.; Zu, Y. Transfecting the Hard-To-Transfect Lymphoma/Leukemia Cells Using a Simple Cationic Polymer Nanocomplex. *J. Controlled Release* **2012**, *159*, 104–110.
29. Zhao, N.; Fogg, J. M.; Zechiedrich, L.; Zu, Y. Transfection of shRNA-Encoding Minivector DNA of a Few Hundred Base Pairs to Regulate Gene Expression in Lymphoma Cells. *Gene Ther.* **2011**, *18*, 220–224.
30. Lukianova-Hleb, E.; Lapotko, D. O. Influence of Transient Environmental Photothermal Effects on Optical Scattering by Gold Nanoparticles. *Nano Lett.* **2009**, *9*, 2160–2166.
31. Lukianova-Hleb, E.; Hu, Y.; Latterini, L.; Tarpani, L.; Lee, S.; Drezek, R. A.; Hafner, J. H.; Lapotko, D. O. Plasmonic Nanobubbles as Transient Vapor Nanobubbles Generated Around Plasmonic Nanoparticles. *ACS Nano* **2010**, *4*, 2109–2123.
32. Wagner, D.; Delk, N.; Lukianova-Hleb, E.; Hafner, J.; Farash-Carson, M. C.; Lapotko, D. The *in Vivo* Performance of Plasmonic Nanobubbles as Cell Theranostic Agents in Zebrafish Hosting Prostate Cancer Xenografts. *Biomaterials* **2010**, *31*, 7567–7574.
33. Lukianova-Hleb, E.; Hanna, E. Y.; Hafner, J. H.; Lapotko, D. O. Tunable Plasmonic Nanobubbles for Cell Theranostics. *Nanotechnology* **2010**, *21*, 085102.
34. Lukianova-Hleb, E.; Ren, X.; Constantinou, P.; Danysh, B.; Shenefelt, D.; Carson, D.; Farach-Carson, M.; Kulchitsky, V.; Wu, X.; Wagner, D.; *et al*. Improved Cellular Specificity of Plasmonic Nanobubbles *Versus* Nanoparticles in Heterogeneous Cell Systems. *PLos One* **2012**, *7*, e34537.
35. Lukianova-Hleb, E.; Samaniego, A.; Wen, J.; Metelitsa, L.; Chang, C.-C.; Lapotko, D. Selective Gene Transfection of Individual Cells *in Vitro* with Plasmonic Nanobubbles. *J. Controlled Release* **2011**, *152*, 286–293.
36. Norman, D. J.; Leone, M. R. The Role of OKT3 in Clinical Transplantation. *Pediatr. Nephrol.* **1991**, *5*, 130–136.
37. Richards, J.; Auger, J.; Peace, D.; Gale, D.; Michel, J.; Koons, A.; Haverty, T.; Zivin, R.; Jolliffe, L.; Bluestone, J. A. Phase I Evaluation of Humanized OKT3: Toxicity and Immunomodulatory Effects of hOKT3gamma4. *Cancer Res.* **1999**, *59*, 2096–2101.
38. Lukianova-Hleb, E. Y.; Ren, X.; Zasadzinski, J. A.; Wu, X.; Lapotko., D. O. Plasmonic Nanobubbles Enhance Efficacy and Selectivity of Chemotherapy Against Drug-Resistant Cancer Cells. *Adv. Mater.* **2012**, *24*, 3831–3837.
39. Lukianova-Hleb, E.; Wagner, D.; Brenner, M.; Lapotko, D. Cell-Specific Transmembrane Injection of Molecular Cargo with Gold Nanoparticle-Generated Transient Plasmonic Nanobubbles. *Biomaterials* **2012**, *33*, 5441–5450.
40. Lapotko, D. O.; Lukianova, E.; Oraevsky, A. A. Selective Laser Nano-Thermolysis of Human Leukemia Cells with Microbubbles Generated Around Clusters of Gold Nanoparticles. *Lasers Surg. Med.* **2006**, *38*, 631–642.
41. Lukianova-Hleb, E. Y.; Belyanin, A.; Kashinath, S.; Wu, X.; Lapotko, D. Plasmonic Nanobubble-Enhanced Endosomal Escape Processes for Selective and Guided Intracellular Delivery of Chemotherapy to Drug-Resistant Cancer Cells. *Biomaterials* **2012**, *33*, 1821–1826.
42. Lapotko, D.; Lukianova-Hleb, E.; Oraevsky, A. Clusterization of Nanoparticles during Their Interaction with Living Cells. *Nanomedicine* **2007**, *2*, 241–253.
43. Mueller, H.; Kassack, M. U.; Wiese, M. Comparison of the Usefulness of the MTT, ATP, and Calcein Assays to Predict the Potency of Cytotoxic Agents in Various Human Cancer Cell Lines. *J. Biomol. Screen.* **2004**, *9*, 506–15.
44. Balazs, D. A.; Godbey, W. T. Liposomes for Use in Gene Delivery. *J. Drug Delivery* **2011**, *2011*, 326497.
45. Shukla, S.; Kavak, E.; Gregory, M.; Imashimizu, M.; Shutinoski, B.; Kashlev, M.; Oberdoerffer, P.; Sandberg, R.; Oberdoerffer, S.

CTCF-Promoted RNA Polymerase II Pausing Links DNA Methylation to Splicing. *Nature* **2011**, *479*, 74–81.
46. Gaspar, V. M.; Correia, I. J.; Sousa, A.; Silva, F.; Paquete, C. M.; Queiroz, J. A.; Sousa, F. Nanoparticle Mediated Delivery of Pure p53 Supercoiled Plasmid DNA for Gene Therapy. *J. Controlled Release* **2011**, *156*, 212–222.
47. Pissuwan, D.; Niidome, T.; Cortie, M. B. The Forthcoming Applications of Gold Nanoparticles in Drug and Gene Delivery Systems. *J. Controlled Release* **2011**, *149*, 65–71.
48. Jain, P. K.; Huang, X.; El-Sayed, I. H.; El-Sayed, M. A. Noble Metals on the Nanoscale: Optical and Photothermal Properties and Some Applications in Imaging, Sensing, Biology, and Medicine. *Acc. Chem. Res.* **2008**, *41*, 1578–1586.
49. Braun, G. B.; Pallaoro, A.; Wu, G.; Missirlis, D.; Zasadzinski, J. A.; Tirrell, M.; Reich, N. O. Laser-Activated Gene Silencing *via* Gold Nanoshell-siRNA Conjugates. *ACS Nano* **2009**, *3*, 2007–2015.
50. Baldi, L.; Hacker, D. L.; Meerschman, C.; Wurm, F. M. Large-Scale Transfection of Mammalian Cells. In *Protein Expression in Mammalian Cells: Methods and Protocols, Methods in Molecular Biology*; Hartley, J. L., Ed.; Humana Press: New York, 2012; Vol. 801, pp 64−74.
51. Bédard, M. F.; Braun, D.; Sukhorukov, G. B.; Skirtach, A. G. Toward Self-Assembly of Nanoparticles on Polymeric Microshells: Near-IR Release and Permeability. *ASC Nano* **2008**, *2*, 1807–1816.
52. Delcea, M.; Sternberg, N.; Yashchenok, A. M.; Georgieva, R.; Bäumler, H.; Möhwald, H.; Skirtach, A. G. Nanoplasmonics for Dual-Molecule Release Through Nanopores in the Membrane of Red Blood Cells. *ACS Nano* **2012**, *6*, 4169–4180.
53. Skirtach, A. G.; Dejugnat, C.; Braun, D.; Susha, A. S.; Rogach, A. L.; Parak, W. J.; Möhwald, H.; Sukhorukov, G. B. The Role of Metal Nanoparticles in Remote Release of Encapsulated Materials. *Nano Lett.* **2005**, *5*, 1371–1377.
54. Wu, G.; Mikhailovsky, A.; Khant, H. A.; Zasadzinski, J. A. Chapter 14: Synthesis, Characterization, and Optical Response of Gold Nanoshells Used To Trigger Release From Liposomes. *Methods Enzymol.* **2009**, *464*, 279–307.
55. Mie, G. Beitrage zur Optik Trüber Medien, Speziell Kolloidaler Metallosungen. *Ann. Phys. Leipzig* **1908**, *25*, 377–445.
56. Bohren, C. F.; Huffman, D. R. *Absorption and Scattering of Light by Small Particles*; Wiley Interscience: New York, 1983.
57. Lukianova-Hleb, E. Y.; Volkov, A. N.; Wu, X.; Lapotko, D. O. Transient Enhancement and Spectral Narrowing of the Photothermal Effect of Plasmonic Nanoparticles under Pulsed Excitation. *Adv. Mater.* **2012**, 10.1002/adma.201204083.
58. Lukianova-Hleb, E. Y.; Sassaroli, E.; Jones, A.; Lapotko, D. O. Transient Photothermal Spectra of Plasmonic Nanobubbles. *Langmuir* **2012**, *28*, 4858–4866.